Article

Structural Models and Atomic Distribution of Bimetallic Nanoparticles as Investigated by X-ray Absorption Spectroscopy

Bing-Joe Hwang, Loka Subramanyam Sarma, Jiun-Ming Chen, Ching-Hsiang Chen, Shou-Chu Shih, Guo-Rung Wang, Din-Goa Liu, Jyh-Fu Lee, and Mau-Tsu Tang

J. Am. Chem. Soc., **2005**, 127 (31), 11140-11145• DOI: 10.1021/ja0526618 • Publication Date (Web): 16 July 2005

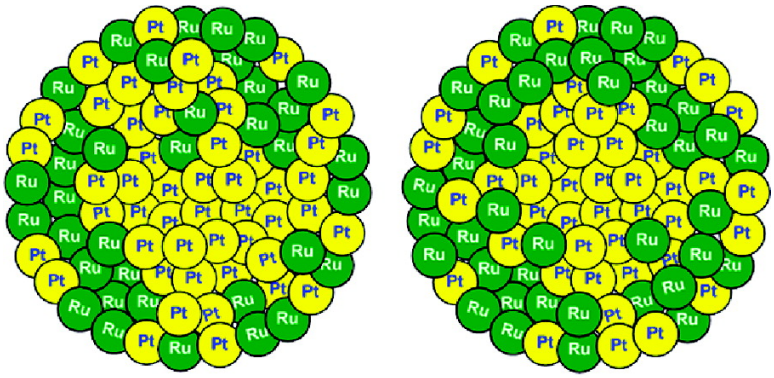

More About This Article

Additional resources and features associated with this article are available within the HTML version:

- Supporting Information
- Links to the 16 articles that cite this article, as of the time of this article download
- Access to high resolution figures
- Links to articles and content related to this article
- Copyright permission to reproduce figures and/or text from this article

View the Full Text HTML

J|A|C|S
ARTICLES
Published on Web 07/16/2005

Structural Models and Atomic Distribution of Bimetallic Nanoparticles as Investigated by X-ray Absorption Spectroscopy

Bing-Joe Hwang,*,† Loka Subramanyam Sarma,† Jiun-Ming Chen,† Ching-Hsiang Chen,† Shou-Chu Shih,† Guo-Rung Wang,† Din-Goa Liu,‡ Jyh-Fu Lee,‡ and Mau-Tsu Tang‡

Contribution from the Nanoelectrochemistry Laboratory, Department of Chemical Engineering, National Taiwan University of Science and Technology, Taipei 106, Taiwan, Republic of China, and National Synchrotron Radiation Research Center, Hsinchu 300, Taiwan

Received April 25, 2005; E-mail: bjh@mail.ntust.edu.tw

Abstract: In this report, we describe a general methodology to determine the extent of alloying or atomic distribution quantitatively in bimetallic nanoparticles (NPs) by X-ray absorption spectroscopy (XAS). The structural parameters determined in these studies serve as a quantitative index and provide a general route to determine the structural aspects of the bimetallic NPs. We have derived various types of possible structural models based on the extent of alloying and coordination number parameters of bimetallic NPs. We also discussed the nature of homo- and heterometallic interactions in bimetallic NPs based on the extent of alloying. Herein, we use carbon-supported platinum−ruthenium bimetallic nanoparticles to demonstrate the proposed methodology, and this can be extended further to get more insights into the alloying extent or atomic distribution of other bimetallic systems. The results demonstrated in this paper open up methods to determine the atomic distribution of bimetallic NPs, which is an extremely important parameter that strongly influences the physicochemical properties of NPs and their applications.

1. Introduction

Bimetallic nanoparticles (NPs) are of great interest from both a scientific and a technological perspective because the addition of the second metal provides a method to control chemical and physical properties.[1,2] Bimetallic NPs have been widely exploited for use in catalysis,[3−5] optoelectronics,[6] information storage,[7−9] biological labeling,[10] and they are prospective substrates for surface-enhanced Raman scattering (SERS).[11,12] The physicochemical properties of nanoparticles depend on several factors, to mention a few such as (i) the particle homogeneity; (ii) the surface segregation of the particles; (iii) the structure and shape of the particles; and (iv) the extent of alloying or atomic distribution in bimetallic NPs.

It has been fairly observed that our knowledge of the catalytic reaction mechanisms will be improved if we can relate the catalytic activity to the structural aspects of the materials[13] because most of the catalytic reactions are structure sensitive, and hence methods to get more insights into structural aspects are highly needed. Of interest is to control the homogeneity, dispersion, alloying extent, and structure as they have profound influence on the surface properties which affect the catalytic activity, selectivity, and stability of the bimetallic nanoparticles. Even though alloying is a well-known phenomenon, detailed studies on quantitative assessment of alloying extent or atomic distribution in bimetallic NPs have been lacking so far. Hence, it is of great interest to search for methods which can precisely estimate the atomic distribution or extent of alloying in bimetallic nanoparticles. The theoretical investigations based on Monte Carlo simulation and density functional theory methods are supposed to estimate the metallic interactions, segregation effects, and atomic distribution of particles in bimetallic nanoparticles. For example, Wang et al. have described the segregation behavior in Pt−Ni catalyst nanoparticles[14] and in Pt−Re bimetallic nanoparticles[15] by using Monte Carlo simulation methods. Due to the constraints that exist in

† National Taiwan University of Science and Technology.
‡ National Synchrotron Radiation Research Center, Hsinchu 300, Taiwan.

(1) Sinfelt, J. H. *Bimetallic Catalysts: Discoveries, Concepts, and Applications*: *Exxon Monograph*; Wiley: New York, 1983.
(2) Sinfelt, J. H. *Acc. Chem. Res.* **1987**, *20*, 134−139.
(3) He, J.; Ichinose, I.; Kunitake, T.; Nako, A.; Shirashi, Y.; Toshima, N. *J. Am. Chem. Soc.* **2003**, *125*, 11034−11040.
(4) Zhou, B.; Hermans, S.; Somorjai, G. A. *Nanotechnology in Catalysis*; Kluwer Academic/Plenum Publishers: New York, 2004.
(5) Thomas, J. M.; Johnson, B. F.; Raja, R.; Sankar, G.; Midgley, P. A. *Acc. Chem. Res*. **2003**, *36*, 20−30.
(6) Kamat, P. V. *J. Phys. Chem. B* **2002**, *106*, 7729−7744.
(7) Sun, S.; Murray, C. B.; Weller, D.; Folks, L.; Moser, A. *Science* **2000**, *287*, 1989−1992.
(8) Christodoulides, J. A.; Huang, Y.; Zhang, Y.; Hadjipanayis, G. C.; Panagiotopoulos, I.; Niarchos, D. *J. Appl. Phys.* **2000**, *87*, 6938−6940.
(9) Park, J., II; Kim, M. G.; Jun, Y.-W.; Lee, J. S.; Lee, W.-R.; Cheon, J. *J. Am. Chem. Soc*. **2004**, *126*, 9072−9078.
(10) Nicewarner-Peña, S. R.; Freemann, R. G.; Reiss, B. D.; He, L.; Peña, D.; Walton, I. D.; Cromer, R.; Keating, C. D.; Natan, M. J. *Science* **2001**, *294*, 137−141.
(11) Freeman, R. G.; Hommer, M. B.; Grabar, K. C.; Jackson, M. A.; Natan, M. J. *J. Phys. Chem*. **1996**, *100*, 718−724.
(12) Lu, P.; Dong, J.; Toshima, N. *Langmuir* **1999**, *15*, 7980−7992.
(13) Somorjai, G. A.; McCrea, K. *Appl. Catal. A: Gen.* **2001**, *222*, 3−18.
(14) Wang, G.; Van Hove, M. A.; Ross, P. N.; Baskes, M. I. *J. Chem. Phys.* **2005**, *122*, 024706.
(15) Wang, G.; Van Hove, M. A.; Ross, P. N.; Baskes, M. I. *J. Chem. Phys.* **2004**, *121*, 5410−5422.

10.1021/ja0526618 CCC: $30.25

choosing the number of atoms used in the simulation process, it is hard to predict the structure and atomic distribution of NPs with the so-called theoretical methods. Also, the theoretical prediction that the bimetallic systems have reached the thermodynamic equilibrium is not accessible during real-time synthesis of NPs. Although it is of immense importance to control or examine the structure and atomic distribution of NPs, predicting them is too difficult from computational and thermodynamic aspects. Meanwhile, most of the synthesis conditions for NPs are not at thermodynamic equilibrium. Differences in atomic distribution, depending on the preparation conditions, even in the case of bimetallic NPs having similar compositions, will have strong influence on their catalytic properties. Hence, it is of great importance to explore a method which can estimate the structure models and atomic distribution of NPs which is most beneficial for physicochemical properties and their applications.

The commonly available X-ray diffraction (XRD) technique to understand the alloy structure of bimetallic nanoparticles may not give real structural information. It lacks the ability to identify short-range ordering (local environment) and only provides information about the long-range ordering and periodicities preferably on single crystals or polycrystals, and hence, conclusions about the alloy structure of nanosized particles cannot be simply drawn from XRD. For example, even though some of the nanoscale Pt−Ru catalysts contain Pt metal, Pt hydrous oxides, Ru hydrous oxides, and Ru metal phases, the XRD technique misidentifies these catalysts and shows that the catalysts contain PtRu alloy phases.[16] The electron microscopy techniques, such as TEM[17,18] and HRTEM,[19,20] will provide only qualitative understanding of the structure of bimetallic nanoparticles. For example, the HRTEM method enables one to distinguish core/shell structure on the basis of observing different lattice spacing. On the other hand, TEM emphasizes the intensity contrast in understanding the structure of bimetallic nanoparticles. The surface-sensitive techniques, such as X-ray photoelectron spectroscopy (XPS),[21] Auger electron spectroscopy (AES),[22] and infrared spectroscopy (IR),[23] are more suitable to realize the surface alloying behavior and segregation phenomena. However, these techniques are not suitable for studying the alloying extent that we are interested in addressing here. Regarding the bimetallic cluster, both anomalous wide-angle X-ray scattering[24−26] (AWAXS) and X-ray absorption spectroscopy (XAS) techniques can provide information on the morphology of the considered species, as well as the distribution of the two metals inside the species.

With the development of XAS, researchers have obtained a tool which is particularly well suited for the structural investigation of bimetallic NPs. XAS studies at both the near-edge X-ray absorption spectroscopy (XANES) region (conventionally from below the edge up to ∼30−50 eV) and the extended X-ray absorption fine structure (EXAFS) region (above the edge ∼30−50 eV), either the L-edge[27] or the K-edge[28] of transition metals, has proved to be an invaluable tool for in situ structural studies[29,30] of nanoparticles and has wide applications.[31−33]

The XANES spectra provide information about the oxidation state, fractional d-electron density, and electronic environment of the absorbing atom, while the EXAFS spectra yield information on the number, type, and distance of the backscattering atom surrounding the central absorbing atom and allow investigations on the short-range ordering and provide geometric information. In recent years, XAS studies have been well explored on bimetallic nanoparticles.[34−39] However, XAS studies focusing on estimation of atomic distributions or alloying extent in the NPs are limited. In this regard, herein, we attempt to propose a general methodology to estimate the structural characteristics, such as alloying extent or atomic distribution in bimetallic nanoparticles, by deriving the structural parameters from XAS analysis and to demonstrate the results on two commercially available carbon-supported Pt−Ru nanoparticles. We believe that the recipe given herein will be useful to deduce the structures and alloying extent or atomic distribution of other related NP systems.

2. Experimental Section

Catalysts and Sample Preparation. Two commercial Pt−Ru/C catalysts, a 20% Pt/10% Ru supplied by E-TEK and a 20% Pt/10% Ru supplied by Johnson-Matthey, both with a Pt/Ru atomic ratio of 1:1 and with an average particle size of 2−3 nm, were examined in this study. Both of the catalysts were subjected to a 30 min reduction at 298 K under flowing H_2. The catalyst-containing sample was pressed into a pellet in a stainless steel holder using a hydraulic pellet press and used to collect the X-ray absorption data.

XAS Measurements. The X-ray absorption spectra were recorded at the Beam Line BL12B2 at the Spring-8, Hyogo, Japan. The electron storage ring was operated at 8 GeV. A double Si(111) crystal monochromator was employed for energy selection. Three gas-filled ionization chambers were used in series to measure the intensities of the incident beam (I_0), the beam transmitted by the sample (I_t), and the beam subsequently transmitted by the reference foil (I_r). The third ion chamber was used in conjunction with the reference sample, which was a Pt foil for Pt L_{III}-edge measurements and Ru powder for Ru K-edge measurements. The stainless steel holder containing the sample was placed between the incident beam detector and the reference beam

(16) Rolison, D. R.; Hagans, P. L.; Swider, K. E.; Long, J. W. *Langmuir* **1999**, *15*, 774−779.
(17) Srnová-Šloufová, I.; Lednický, F.; Gemperle, A.; Gemperlová, J. *Langmuir* **2000**, *16*, 9928−9935.
(18) Chen, Y. H.; Nickel, U. *J. Chem. Soc., Faraday Trans.* **1993**, *89*, 2479−2485.
(19) Schmid, G. *Clusters and Colloids*; VCH: Weinheim, Germany, 1994.
(20) Link, S.; Wang, Z. L.; El-Sayed, M. A. *J. Phys. Chem. B* **1999**, *103*, 3529−3533.
(21) Polak, M.; Rubinovich, L. *Surf. Sci. Rep.* **2000**, *38*, 127−194.
(22) Batista, J.; Pintar, A.; Ěeh, M. *Catal. Lett.* **1997**, *43*, 79−84.
(23) Huifang, L.; Stephen, M.; Keith, J. S.; Chandler, B. D. *J. Am. Chem. Soc.* **2004**, *126*, 12949−12956.
(24) Waseda, Y. *Novel Application of Anomalous X-ray Scattering for Structural Characterization of Disordered Material*; Springer-Verlag: New York, 1984.
(25) Bazin, D.; Sayers, D. *Jpn. J. Appl. Phys.* **1993**, *32*, 251.
(26) Shido, T.; Prins, R. *Curr. Opin. Solid State Mater. Sci.* **1998**, *3*, 330−335.
(27) Ankudinov, A. L.; Rehr, J. J.; Low, J.; Bare, S. R. *Phys. Rev. Lett.* **2001**, *86*, 1642−1645.
(28) Bazin, D.; Rehr, J. J. *J. Phys. Chem. B* **2003**, *107*, 12398−12402.
(29) Lynch, J. *Oil Gas Sci. Technol.* **2002**, *57*, 281−305.
(30) Grunwaldt, J.-D.; Caravati, M.; Hannemann, S.; Baiker, A. *Phys. Chem. Chem. Phys.* **2004**, *6*, 3037−3047.
(31) Tsai, Y.-W.; Tseng, Y.-L.; Sarma, L. S.; Liu, D.-G.; Lee, J.-F.; Hwang, B.-J. *J. Phys. Chem. B* **2004**, *108*, 8148−8152.
(32) Hwang, B.-J.; Tsai, Y.-W.; Sarma, L. S.; Chen, C.-H.; Lee, J.-F.; Strehblow, H. H. *J. Phys. Chem. B* **2004**, *108*, 15096−15102.
(33) Hwang, B.-J.; Tsai, Y.-W.; Sarma, L.-S.; Liu, D.-G.; Lee, J.-F. *J. Phys. Chem. B* **2004**, *108*, 20427−20434.
(34) Nashner, M. S.; Frenkel, A. I.; Adler, D. L.; Shapley, J. R.; Nuzzo, R. G. *J. Am. Chem. Soc.* **1997**, *119*, 7760−7771.
(35) Nashner, M. S.; Frenkel, A. I.; Somerville, D.; Wills, C. W.; Shapley, J. R.; Nuzzo, *R. G. J. Am. Chem. Soc.* **1998**, *120*, 8093−8101.
(36) Hills, C. W.; Nashner, M. S.; Frenkel, A. I.; Shapley, J. R.; Nuzzo, R. G. *Langmuir* **1999**, *15*, 690−700.
(37) Toshima, N.; Harada, M.; Yamazaki, Y.; Asakura, K. *J. Phys. Chem.* **1992**, *96*, 9927−9933.
(38) Toshima, N.; Harada, M.; Yonezawa, T.; Kushihashi, K.; Asakura, K. *J. Phys. Chem.* **1991**, *95*, 7448−7453.
(39) Bian, C.-R.; Suzuki, S.; Asakura, K.; Ping, L.; Toshima, N. *J. Phys. Chem. B* **2002**, *106*, 8587−8598.

detector. Prior to the XAS measurements, the catalyst sample in the holder was treated with pure H_2 gas for 30 min with a flow rate of 30 cm^3 H_2/min, and then we performed the XAS scan. The sample preparation, control of parameters for EXAFS measurements, and data collection modes are all done as per the guidelines set by International XAFS Society Standards and Criteria Committee.[40,41]

XAS Data Analysis. Standard procedures were followed to analyze the XAS data. First, the raw absorption spectrum in the pre-edge region was fitted to a straight line, and the background above the edge was fitted with a cubic spline. The EXAFS function, χ, was obtained by subtracting the post-edge background from the overall absorption and then normalized with respect to the edge jump step. The normalized $\chi(E)$ was transformed from energy space to k-space, where k is the photoelectron wave vector. The $\chi(k)$ data were multiplied by k^2 to compensate for the damping of EXAFS oscillations in the high k-region. Subsequently, k^2-weighted $\chi(k)$ data in the k-space ranging from 3.6 to 12.5 $Å^{-1}$ for the Pt L_{III}-edge and from 3.6 to 11.6 $Å^{-1}$ for the Ru K-edge were Fourier transformed (FT) to r-space to separate the EXAFS contributions from the different coordination shells. A nonlinear least-squares algorithm was applied to the curve fitting of an EXAFS in the r-space between 1.7 and 3.2 Å (without phase correction) for Pt and between 1.5 and 3.3 Å for Ru. The Pt−Ru reference file was determined by a theoretical calculation. All of the computer programs were implemented in the UWXAFS 3.0 package[42] with the backscattering amplitude and the phase shift for the specific atom pairs being theoretically calculated by using FEFF7 code.[43] From these analyses, structural parameters, such as coordination numbers (N), bond distance (R), the Debye−Waller factor ($\Delta\sigma_j^2$), and inner potential shift (ΔE_0), have been calculated.

CO Stripping Voltammetry. A CO voltammetric stripping experiment was performed as follows. CO was adsorbed onto the electrode surface at 0.1 V versus NHE by bubbling the high-purity CO gas through the 0.5 M H_2SO_4 solution for 15 min. The CO adsorption time was found to be sufficient to reach the steady state. CO stripping was studied after flushing the cell with N_2 for 15 min while still holding the potential at 0.1 V versus NHE. Then the potential was scanned from 0.2 to 1.2 V versus NHE at 5 mV/s to record the CO stripping voltammograms.

3. Results and Discussion

The structure of bimetallic nanoparticles (NPs), which contains two kinds of metal elements, may possess the crystal structure similar either to the bulk alloy or another type in which the distribution of each metal element is different from the bulk. In the literature, many reports have appeared describing the applicability of XAS to derive the structural models for bimetallic NPs.[37−39,44] However, researchers have proposed only qualitatively the structural models of bimetallic NPs, such as random alloy, alloy with an intermetallic compound type, cluster-in-cluster, and core−shell structure.[44] Literature describing the quantitative extent of alloying or atomic distribution of bimetallic NPs is rather scarce. It is of interest to estimate the extent of alloying or atomic distribution of elements in bimetallic NPs to get more insights into the structure, as well as their real applications. In this direction, we have analyzed the bimetallic NPs (of types A−B) by XAS. By estimating the ratio of the coordination number of A around B and also the coordination number of B around A to the total coordination numbers, we have deduced the quantitative parameters, J_A and J_B, for the alloying extent in A−B bimetallic NPs, and the meaning of these parameters will be described in the following paragraph.

The quantitative extent of alloying or atomic distribution in bimetallic NPs can be evaluated by deriving the XAS structural parameters. The parameters that are needed to derive the extent of alloying are represented as $P_{observed}$, $R_{observed}$, P_{random}, and R_{random}. The parameter $P_{observed}$ can be defined as a ratio of the scattering atoms B coordination number around absorbing A atoms (N_{A-B}) to the total coordination number of absorbing atoms ($\sum N_{A-i}$) ($P_{observed} = N_{A-B}/\sum N_{A-i}$). Similarly, $R_{observed}$ can be defined as a ratio of the scattering atoms A coordination number around absorbing B atoms (N_{B-A}) to the total coordination number of absorbing atoms ($\sum N_{B-i}$) ($R_{observed} = N_{B-A}/\sum N_{B-i}$). Whereas, P_{random} and R_{random} can be taken as 0.5 for perfect alloyed bimetallic NPs if the atomic ratio of A and B is 1:1. This value can be achieved by assuming $N_{A-A} = N_{A-B}$ and $N_{B-B} = N_{B-A}$, which is generally true for perfect alloyed bimetallic NPs. This methodology can be easily extended to the other NP systems of interest. For example, in the case of 1:2 bimetallic NPs, $2N_{A-A} = N_{A-B}$ and $N_{B-B} = 2N_{B-A}$ for perfect alloyed bimetallic NPs, indicating that P_{random} and R_{random} would be 0.67 and 0.33, respectively. In the case of 1:4 bimetallic NPs, $4N_{A-A} = N_{A-B}$ and $N_{B-B} = 4N_{B-A}$ for perfect alloyed bimetallic NPs and, therefore, P_{random} and R_{random} can be taken as 0.8 and 0.2, respectively. In this contribution, we will focus on the 1:1 bimetallic NP system. From the ratio of $P_{observed}$ to P_{random}, we can evaluate the extent of alloying of the A element in NPs, and similarly, from the ratio of $R_{observed}$ to R_{random}, we can estimate the alloying extent of the B element in NPs. The extent of alloying of element A (J_A) and element B (J_B) for 1:1 A−B bimetallic NPs can be calculated quantitatively by using the eqs 1 and 2, respectively.

$$J_A = \frac{P_{observed}}{P_{random}} \times 100\% \quad (1)$$

$$J_B = \frac{R_{observed}}{R_{random}} \times 100\% \quad (2)$$

It is possible to construct the structural models emphasizing the atomic distribution in the bimetallic NPs with the knowledge of the $\sum N_{A-i}$, $\sum N_{B-i}$, J_A, and J_B values derived from XAS. With the help of the extent of alloying values and structural parameters extracted from EXAFS, it is possible to predict the structure models of NPs. Herein, we will discuss seven possible cases, and schematic presentation of the corresponding structural models are presented in Figure 1. Even though we present seven cases, in fact, there are unlimited cases possible which really depend on the alloying extent and will influence the behavior of NPs, especially in catalytic applications. In case 1, if $J_A = 0$ and $J_B = 0$, then both A and B particles are not involved in the alloying and resulted in separated cluster particles (see Figure 1, case 1). In this case, if $N_{A-A} = N_{B-B}$, this means that the particle size of both A and B is same, but $N_{A-A} > N_{B-B}$ means the particle size of A is larger than that of B. It is also interesting to discuss the extent of metallic interactions based on the alloy extent of A and B. However, only at the equilibrium state is it possible to know the nature of metallic interactions. For bimetallic NP systems, which have not reached the kinetic

(40) See, for example, the guidelines for data collection modes for EXAFS measurements and user-controlled parameters at http://ixs.iit.edu/subcommittee_reports/sc/sc00report.pdf.
(41) Guidelines for errors reporting can be found at http://ixs.iit.edu/subcommittee_reports/sc/err-rep.pdf.
(42) Stern, E. A.; Newville, M.; Ravel, B.; Yacoby, Y.; Haskel, D. *Physica B* **1995**, *208−209*, 117−120.
(43) Zabinsky, S. I.; Rehr, J. J.; Ankudinov, A. L.; Albers, R. C.; Eller, M. J. *Phys. Rev. B* **1995**, *52*, 2995−3009.

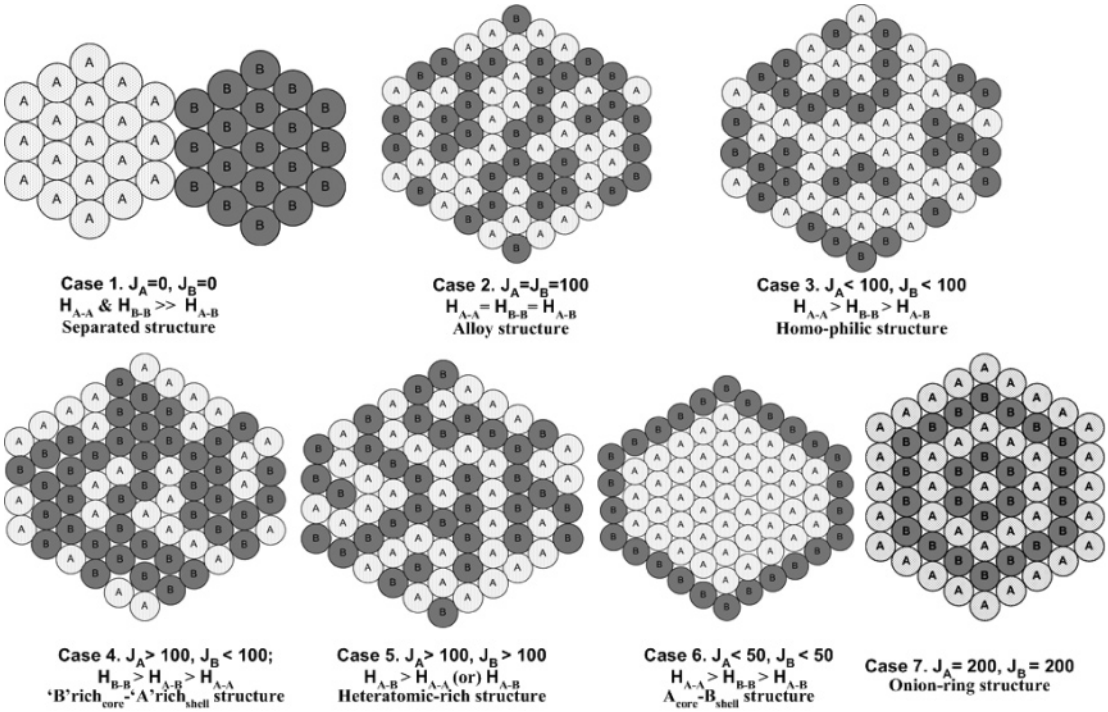

Figure 1. Schematics of bimetallic nanoparticles at various degrees of alloying.

barrier, it is not possible to assess the extent of metallic interactions. If NPs reach the equilibrium state, then we can further discuss the extent of interactions between the atoms in NPs. In this case, homoatomic interaction of A atoms (H_{A-A}) and homoatomic interaction of B atoms (H_{B-B}) $\gg$ bimetallic (A−B) heteroatomic interactions (H_{A-B}) and means that there are no heteroatomic interactions in the NPs. In case 2, if $J_A = J_B = 100\%$, then both the A and B atoms are involved completely in the alloying process and resulted in perfect alloyed NPs (see Figure 1, case 2). If the bimetallic system is in the equilibrium state, then the interactions will be $H_{A-A} = H_{B-B} = H_{A-B}$, which means that there are equal bimetallic interactions in the NPs. In case 3, if $J_A < 100\%$ and $J_B < 100\%$, then both A and B atoms are not preferred to be alloyed, and it indicates that a higher extent of A/B atoms prefer A/B atoms and prefer only to a lesser extent alloying between A and B atoms. If $J_B > J_A$, it appears that the core is rich in A atoms and the shell is rich in B atoms (see Figure 1, case 3). Here, it is noteworthy to discuss the coordination number parameters. The $\sum N_{A-i}$ will be greater than that of $\sum N_{B-i}$. At equilibrium conditions, we can see that the order of interactions will be $H_{A-A} > H_{B-B} > H_{A-B}$. On the contrary, if $J_A > J_B$, then in the resulting bimetallic NPs, B atoms are rich in the core and A atoms are rich in the shell (model not shown in the figure). In this case, $\sum N_{B-i} > \sum N_{A-i}$. At the equilibrium state, the interaction follows the order $H_{B-B} > H_{A-A} > H_{A-B}$. In case 4, if $J_A > 100\%$ and $J_B < 100\%$, then B atoms prefer B atoms rather than A, and A atoms prefer B atoms rather than A atoms. As a result, atomic distribution of A atoms is better than that of B atoms. In other words, we can say that the segregation of A atoms is less pronounced than that of B atoms. At the equilibrium state, the interactions are in the following order: $H_{B-B} > H_{A-B} > H_{A-A}$. In this type, the bimetallic NPs adopt a structure similar to that of the B rich in core−A rich in shell (see Figure 1, case 4). Here, the $\sum N_{B-i} > \sum N_{A-i}$. Even though the structures described in cases 3 and 4 are similar in nature, the atomic dispersion of A atoms in the NPs of case 4 is better, indicating the J_A role in providing the degree of atomic dispersion in NPs quantitatively, which we cannot simply obtain from the coordination numbers. If $J_A < 100\%$ and $J_B > 100\%$, the situation is opposite to the case 4, that is, the atomic distribution of B atoms is better when compared to that of A atoms. As a result, the structure will be similar to that of the A rich in core−B rich in shell (model not shown in the figure). At the equilibrium state, the interactions are in the order $H_{A-A} > H_{A-B} > H_{B-B}$. In case 5, if $J_A > 100\%$ and $J_B > 100\%$, then the atomic distribution of both A and B atoms is improved, and in the resulting structure, we can expect more heteroatomic interactions than homoatomic interactions (see Figure 1, case 5). At equilibrium, the interactions will be in the following order: $H_{A-B} > H_{A-A}$ and $H_{A-B} > H_{B-B}$. By comparing the different models described above (from cases 3−5), we can provide quantitative atomic distribution, which can be very important for NP applications. In case 6, if $J_A < 50\%$ and $J_B < 50\%$, then the resultant structure A particles are in the core and B particles are in the shell (see Figure 1, case 6). The total coordination number, $\sum N_{A-i}$, will be greater than that of $\sum N_{B-i}$. At the equilibrium state, the interactions follows the order $H_{A-A} > H_{B-B} > H_{A-B}$. If $J_A < 50\%$ and $J_B < 50\%$, the bimetallic NPs adopt a structure similar to that of the B core−A shell model (model not shown in the figure). In this case, $\sum N_{B-i} > \sum N_{A-i}$, and the interactions at equilibrium state are in the following order: $H_{B-B} > H_{A-A} > H_{A-B}$. In case 7, if $J_A = 200\%$ and $J_B = 200\%$, then A atoms always prefer B atoms and vice versa, and the resulting structure looks like an onion ring (see Figure 1, case 7), in which one layer is occupied by A atoms and the other layer by B atoms.

By using the above-mentioned eqs 1 and 2, we have derived the alloying extent quantitatively in commercial E-TEK 30 and JM30 Pt−Ru/C nanoparticles (see Table 1). The EXAFS oscillations in the background-subtracted k^2-weighted spectra recorded at the Pt L_{III}-edge and at Ru K-edge (Figure S1) and their corresponding Fourier transforms (Figure S2), EXAFS

Table 1. Structural Coordination Number Parameters and Alloying Extent for Commercial E-TEK 30 and JM 30 Pt−Ru/C NPs and for Some Other 1:1 Bimetallic NPs Reported in the Literature

NPs	N_{A-B}	N_{B-A}	N_{A-i}	N_{B-i}	$P_{observed}$	$R_{observed}$	J_A (%)	J_B (%)	structure models
					JM 30				
(A = Pt, B = Ru)	1.4	2.2	7.0	5.6	0.20	0.39	40	78	Pt $rich_{core}$−Ru $rich_{shell}$ (Figure 2a)
					E-TEK 30				
(A = Pt, B = Ru)	0.9	1.2	7.1	4.9	0.13	0.24	26	48	Pt $rich_{core}$−Ru $rich_{shell}$ (Figure 2b)
					Pd−Au (1:1)[a]				
(A = Pd, B = Au)	2.5	2.3	4.0	8.8	0.62	0.26	125	52	Au $rich_{core}$−Pd $rich_{shell}$ (Figure 1, case 4)
					Pd−Pt (1:1)[b]				
(A = Pd, B = Pt)	3.0	1.3	5.3	6.1	0.57	0.21	113	43	Pt $rich_{core}$−Pd $rich_{shell}$ (Figure 1, case 4)
					Cu−Pd (1:1)[c]				
(A = Cu, B = Pd)	5.0	5.1	7.8	7.9	0.64	0.64	128	129	Heteroatomic-rich (Figure 1, case 5)

[a] See ref 37. [b] See ref 38. [c] See ref 39.

parameters such as bond distance (R), the Debye−Waller factor ($\Delta\sigma_j^2$), and inner potential shift (ΔE_0) (Table S1) have been provided in the Supporting Information. We also calculated the quantitative extent of alloying for some of the 1:1 bimetallic NP systems reported in the literature by using the derived equation (See Table 1)

We have employed the derived expressions for J_A and J_B from the coordination numbers of bimetallic NPs reported in the literature[37−39] and compared in Table 1.

On the basis of the alloying extent, we have checked the reliability of the structural models that are suggested for the bimetallic NPs. It is quite interesting that, if we apply our derived expression for J_A and J_B to calculate the alloying extent of Au and Pd, respectively, for a 1:1 Au−Pd bimetallic NP,[37] we have achieved the values $J_{Pd} = 125$ and $J_{Au} = 52$. It indicates that Au atoms are rich in the core and Pd atoms are rich in the shell, similar to the model shown in Figure 1, case 4. From the J_{Pd} and J_{Au} values, we can understand that the atomic dispersion of Pd is better than the atomic dispersion of Au in the Au−Pd bimetallic NPs. Similarly, if we apply our methodology to calculate the alloying extent of Pd and Pt for a 1:1 Pd−Pt bimetallic NP,[38] we have found $J_{Pd} = 113$ and $J_{Pt} = 43$. These values suggest that Pd−Pt bimetallic NPs also have a structure similar to the one shown in Figure 1, case 4, in which Pt atoms are rich in the core and Pd atoms are rich in the shell, with a higher extent of Pd atomic dispersion in the NPs. The application of the proposed methodology to Cu−Pd (1:1) bimetallic NPs[39] yields $J_{Pd} = 128$ and $J_{Cu} = 129$, indicating that NPs have an equal extent of Pd and Cu atomic dispersion. The structure model proposed in Figure 1, case 5, suits well for the Cu−Pd (1:1) bimetallic NPs. It is satisfactory that the structural models proposed here based on the alloying extent values agree well with those reported in the literature.

However, in the literature, the structural models proposed for the bimetallic 1:1 Au−Pd, Pd−Pt, and Cu−Pd NPs are drawn only based on the total coordination numbers, $\sum N_{A-i}$ and $\sum N_{B-i}$, and cannot disclose the different degree of atomic distribution precisely. Hence, we believe it is only a qualitative assessment of the structure and needs to consider the extent of alloying or atomic dispersion when predicting the structure of bimetallic NPs. In this way, our investigations will be helpful to estimate quantitatively the extent of atomic distribution or alloying of bimetallic NPs to get more insights into the structure.

Discussion of the Structural Models Proposed for JM 30 and E-TEK 30 Pt−Ru/C Catalysts. The coordination numbers and the extent of alloying of Pt, J_{Pt} (calculated from expression 1), and Ru, J_{Ru} (calculated from expression 2), values for E-TEK 30 and JM30 Pt−Ru/C catalysts are given in Table 1. In the case of JM 30 catalyst, the coordination numbers of Pt and Ru atoms around the Pt atom are found to be 5.6 ± 0.3 and 1.4 ± 0.1, respectively, and the total coordination number $\sum N_{Pt-i}$ is 7.0. The coordination numbers of Ru and Pt atoms around the Ru atom are determined to be 3.4 ± 0.2 and 2.2 ± 0.3, respectively, and the total coordination number $\sum N_{Ru-i}$ is calculated as 5.6. From these values, $P_{observed}$ and $R_{observed}$ are determined to be 0.20 and 0.39, respectively, and J_{Pt} and J_{Ru} values are calculated to be 40 and 78%, respectively. For E-TEK 30 catalyst, we have calculated the coordination numbers of Pt and Ru atoms around the Pt atom to be 6.2 ± 0.3 and 0.9 ± 0.1, respectively, and $\sum N_{Pt-i}$ as 7.1; the coordination numbers of Ru and Pt atoms around the Ru atom are determined to be 3.7 ± 0.2 and 1.2 ± 0.2, respectively, and the $\sum N_{Ru-i}$ as 4.9. The other two structural parameters, $P_{observed}$ and $R_{observed}$, in the case of E-TEK 30 are calculated to be 0.13 and 0.24, respectively, and the J_{Pt} and J_{Ru} values are calculated as 26 and 48%, respectively. It is clear from the structural coordination parameter values of both catalysts that $\sum N_{Pt-i} > \sum N_{Ru-i}$ and $J_{Ru} > J_{Pt}$ and indicates that the catalysts adopt a Pt that is rich in the core and a Ru that is rich in the shell structure, and the schematic representation of the structures of the catalysts is given in Figure 2. The observed parameter relationship (i.e., $\sum N_{A-i} > \sum N_{B-i}$ (A = Pt, B = Ru)) for JM30 and E-TEK 30 Pt−Ru/C catalysts is consistent with the relationship $N_{AA} + N_{AB} > N_{BA} + N_{BB}$ for a homogeneous system for which the core of the cluster is composed of N atoms of A (NA) and the surface is made of N atoms of B (NB), the total coordination number ($N_{AA} + N_{AB}$) for the A atom, and greater than the total coordination for the B atoms ($N_{BA} + N_{BB}$).[45,46]

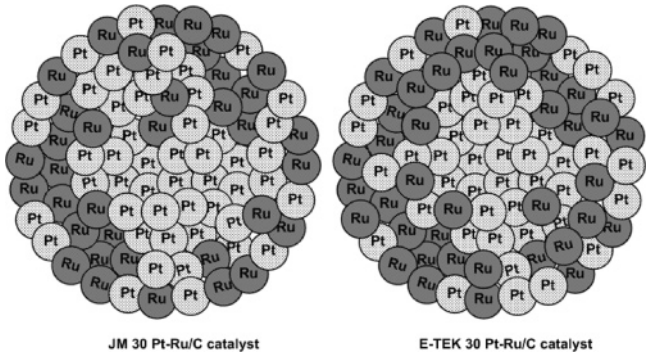

Figure 2. Structural models deduced for JM 30 (a) and E-TEK 30 Pt−Ru/C catalysts (b) based on XAS parameters.

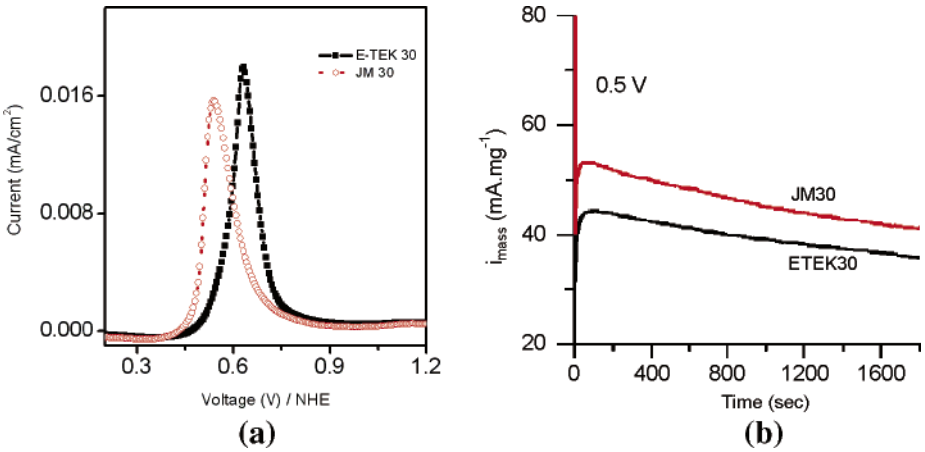

Figure 3. Comparison of methanol oxidation activity of JM 30 and E-TEK 30 Pt−Ru/C catalysts: (a) CO stripping voltammograms recorded in 0.5 M H_2SO_4 solution (CO gas was purged for 15 min at 0.1 V and then stripped); and (b) chronoamperometric analysis at constant potential 0.5 V versus NHE in 15% CH_3OH + 0.5 M H_2SO_4.

From the quantitative extent of alloying values, we can see that in both the catalysts a considerable amount of Ru is segregated on the shell layer, but the extent of segregation of Ru is higher in E-TEK 30 when compared to the JM 30. The increased value of J_{Ru} in the JM 30 catalyst indicated that most of the Ru is involved in alloying and, hence, less segregation of Ru in the shell, whereas in the case of E-TEK 30 catalyst, a lesser extent of Ru is involved in the alloying and considerable extent of segregation of Ru can be expected in the shell region. The segregation of Ru in the case of E-TEK 30, in part, may be responsible for its lower methanol oxidation activity compared to that of JM 30. Recent infrared measurements on the Pt−Ru alloy particle electrodes indicates two modes of adsorbed CO vibrations related to both Pt and Ru domains present on the surface and supports the surface segregation of Ru in commercial catalysts.[47] The results obtained from XAS support the Pt-rich core and Ru-rich shell structure for commercial carbon-supported Pt−Ru catalysts.

Increase in J_{Pt} and J_{Ru} values in JM 30 compared to those of E-TEK 30 indicates that the atomic distribution of Pt and Ru atoms are much facilitated. Increase in atomic distribution can be taken as a measure for enhanced homogeneity. We have performed the CO stripping voltammetry analysis and chronoamperometric analysis on both JM 30 and E-TEK 30 catalysts, and the results are shown in the panels of a and b, respectively, of Figure 3. As can be seen from Figure 3a, CO oxidation on JM 30 starts at lower potentials than on E-TEK 30, indicating its superior oxidation ability. The chronoamperometric analysis presented in Figure 3b also indicates that the highest specific electroactivity was found with the JM 30 catalyst. As far as our XAS analysis is concerned, the enhanced performance of JM 30 can be attributed to its increased extent of alloying or better atomic distribution.

Conclusions

We have shown that the extent of alloying or atomic dispersion in bimetallic nanoparticles can be determined quantitatively from the structural parameters J_A and J_B of A−B bimetallic NPs derived from XAS. From the extent of atomic dispersion or alloying, it is possible to understand and control the structure of bimetallic nanoparticles. We have derived various structural models based on the extent of alloying in bimetallic NPs. These findings are of general interest, and the methodology is convenient for applying to bimetallic NPs prepared under conditions which have not fully reached the thermodynamic equilibrium. Even though we presented discussions on structural models only at some limited cases, the method can be used for an unlimited number of cases that are usually encountered in real-time synthesis of NPs. With the method presented in this paper, we can provide a quantitative index measuring the changes in the atomic distribution, even in the case of bimetallic NPs having similar compositions. The change in the atomic distribution of NPs has great influence on their physicochemical properties, such as the electrocatalytic activity for direct methanol fuel cell (DMFC) applications.

Acknowledgment. The financial support from the National Science Council (NSC92-2811-E−011-001), facilities from the National Synchrotron Radiation Research Center (NSRRC), and the National Taiwan University of Science and Technology, Taiwan, R. O. C is great fully acknowledged.

Supporting Information Available: The k^2-weighted EXAFS spectra, corresponding Fourier transforms, and EXAFS fitting parameters at both Pt L_{III}-edge and Ru K-edge of JM-30 and E-TEK 30 Pt−Ru/C catalysts are provided. This material is available free of charge via the Internet at http://pubs.acs.org.

JA0526618

(44) Toshima, N.; Yonezawa, T. *New J. Chem.* **1998**, *22*, 1179−1201.
(45) Via, G. H.; Sinfelt, J. H. In *X-ray Absorption Fine Structure for Catalysts and Surfaces*; Iwasawa,Y., Ed.; World Scientific: London, 1996.
(46) Bazin, D.; Sayers, D.; Rehr, J. J. *J. Phys. Chem. B* **1997**, *101*, 11040−11050.
(47) Park, S.; Wieckowski, A.; Weaver, M. J. *J. Am. Chem. Soc.* **2003**, *125*, 2282−2290.